Scaleable production of microbubbles using an ultrasound-modulated microfluidic device

Dario Carugo,[1¶] Richard J. Browning,[2,¶] Ida Iranmanesh,[2] Walid Messaoudi,[3] Paul Rademeyer,[2] and Eleanor Stride[2a]

[1] *Department of Pharmaceutics, UCL School of Pharmacy, University College London (UCL), UK*

[2] *Institute of Biomedical Engineering, Department of Engineering Science, University of Oxford, UK*

[3] *Faculty of Engineering and Physical Sciences, University of Southampton, UK*

[¶] *Authors have equally contributed to the work in this study*

Surfactant-coated gas microbubbles are widely used as contrast agents in ultrasound imaging and increasingly in therapeutic applications. The response of microbubbles to ultrasound can be strongly influenced by their size and coating properties and hence the production method. Ultrasonic emulsification (sonication) is the most commonly employed method and can generate high concentrations of microbubbles rapidly, but with a broad size distribution and there is a risk of contamination and/or degradation of sensitive components. Microfluidic devices provide excellent control over microbubble size, but are often challenging or costly to manufacture, offer low production rates ($<10^6 s^{-1}$), and are prone to clogging. In this study, a hybrid sonication-microfluidic or 'sonofluidic' device was developed. Bubbles of ~180 μm diameter were produced rapidly in a T-junction and subsequently exposed to ultrasound (71-73 kHz) within a microchannel, generating microbubbles (mean diameter: 1-2 μm) at a rate of $>10^8 s^{-1}$ using a single device. Microbubbles were prepared using either the sonofluidic device or conventional sonication and their size, concentration and stability compared. The mean diameter, concentration and stability were found to be comparable between techniques, but the microbubbles produced by the sonofluidic device were all <5 μm in diameter and thus did not require any post-production fractionation.

[a] eleanor.stride@eng.ox.ac.uk

I. INTRODUCTION

A. Microbubbles in ultrasound imaging and therapy

In medical imaging, microbubbles are routinely used as ultrasound contrast agents. Their high compressibility enables significant enhancement of ultrasound backscatter from blood by several orders of magnitude. The microbubble core usually consists of a high molecular weight gas (e.g. a perfluorocarbon or sulfur hexafluoride) stabilised by a surfactant or polymer coating (or "shell") to enhance stability during storage, handling, and/or administration (Stride and Saffari 2003). Typical clinical formulations use saturated phospholipids or denatured albumin as the primary shell constituents. Moreover, microbubbles can be loaded with biologically active compounds or functionalised with targeting moieties. This has paved the way for their use as targetable drug delivery systems, whereby the bioactive payload can be released on-demand upon extracorporeal ultrasound stimulation directed to the point of treatment (Ferrara, et al. 2007, Kooiman, et al. 2014).

The clinical utility of microbubbles is profoundly influenced by their physical characteristics, including their average size, size distribution, and the mechanical and rheological properties of the coating layer (Alter, et al. 2009, Garg, et al. 2013, Sirsi, et al. 2010). These characteristics are in turn dependent on the chemical formulation of the microbubble shell and also on the production technique (Al-Jawadi and Thakur 2020, Hosny, et al. 2013). A variety of different methods have been developed for batch production of microbubbles, including ultrasonic emulsification (sonication), high shear emulsification, membrane emulsification, and coaxial electrohydrodynamic atomisation (Stride and Edirisinghe 2008). Sonication is the most commonly employed method in both academic and industrial laboratories, and involves dispersing gas or liquid in a suspension of a coating material using high intensity ultrasound (Stride, et al. 2020). The size distribution of microbubbles obtained from sonication is however relatively broad (Feshitan, et al. 2009) and there is also wide variability in coating properties (Browning, et al. 2019), which may lead to a large variation in acoustic response across a

47 microbubble population (Rademeyer, et al. 2015). Post-production procedures (i.e., fractionation or
48 filtration) are usually required in order to remove large bubbles (i.e., with diameters > 10 μm) that
49 could cause vascular occlusion after intravenous injection, as well as excess coating material not
50 incorporated onto the microbubble (Dewitte, et al. 2019, Feshitan, et al. 2009). The latter is particularly
51 important in the case of drug-loaded microbubbles, to enable accurate quantification of the
52 administered dose.

53 **B. Microfluidic techniques for microbubble production**

54 More recently, microfluidic techniques have been proposed as an alternative to batch methods
55 for producing more uniform microbubbles (Chen, et al. 2014, Dhanaliwala, et al. 2013, Gnyawali, et
56 al. 2017, Hettiarachchi, et al. 2007, Jiang, et al. 2016, Peyman, et al. 2012, Rickel, et al. 2018, Segers, et
57 al. 2020, Seo, et al. 2010, van Elburg, et al. 2021). A typical microfluidic device consists of a cross-flow
58 (i.e., flow focusing) or T-junction architecture, in which gas and liquid streams are forced to flow into
59 a confined microchannel where the gas stream breaks up into individual microbubbles, a process often
60 referred to as 'pinch-off' (Garstecki, et al. 2006, Pahlavan, et al. 2019). Microbubbles produced with
61 this technique typically have a polydispersity index <5%. However, production of microbubbles
62 having clinically applicable diameters (i.e., in the range 1-10 μm) requires microchannel features of
63 comparable dimensions (Hettiarachchi, et al. 2007), which can reduce a device's lifetime considerably
64 (i.e., due to clogging or excessive backpressure). Depending on the geometrical properties of the
65 microchannels and the flow dynamic field, different microbubble production regimes have been
66 demonstrated using these architectures (Dollet, et al. 2008). However, production rates are typically
67 lower compared with batch methods (Table 1), and microbubble stability has also been reported to be
68 lower in some cases (Hosny, et al. 2013). These factors have hindered the adoption of microfluidics
69 for industrial production of microbubbles for clinical usage.

Some of these limitations can be addressed through changes to the operating conditions and/or the device architecture. For example, Peyman *et al.* were able to achieve a micro-spraying microbubble formation regime by varying the geometry of a flow-focusing microfluidic device, specifically by widening the exit channel and introducing an abrupt increase in the channel depth. When compared to a more conventional pinch-off formation regime, micro-spraying resulted in microbubble suspensions having ~100-times greater concentration (i.e., up to 10^9 microbubbles/mL) (Peyman, et al. 2012). However, the size distribution of microbubbles produced by micro-spraying presented comparable relative standard deviation to that of microbubbles produced by batch mechanical agitation; although the latter method generated some microbubbles with diameter >10 μm that were not present in the microfluidic-generated samples. Castro-Hernández *et al.* demonstrated that careful selection of the hydrodynamic boundary conditions in a planar flow-focusing device can enable production of microbubbles with dimensions one order of magnitude smaller than the microchannel width, when the length of the exit channel is designed to be significantly greater than its width (Castro-Hernández, et al. 2011). With this method, microbubbles ~5 μm diameter and with a polydispersity index <5% could be produced at a rate $>10^5$ microbubbles/sec, which represents an improvement compared to more conventional microfluidic systems based on microbubble pinch-off. However, manufacturing of the microchannels in this study still required costly and time-consuming photolithographic techniques, and scaling up production of microbubble suspensions with a mean diameter of 1-3 μm (often employed in therapeutic applications) could pose challenges.

Identifying a microbubble production method that relies on further scaled-up channel architectures (i.e., up to 100s or 1000s of μm) would enable both greater production rates and overcome challenges associated with clogging, high backpressure and manufacturing costs. However, additional modifications to the microbubble production mechanism or the physico-chemical properties of fluidic environment may be required in order to produce microbubbles of clinically

relevant sizes *via* these scaled-up devices. For instance, devices consisting of off-the-shelf capillaries embedded within an easy-to-fabricate T-junction manifold have been previously employed to produce microbubbles (Parhizkar, et al. 2013, Parhizkar, et al. 2015, Parhizkar, et al. 2014). Parhizkar *et al.* employed capillaries with inner diameter in the range 100-200 μm, and investigated the effect of varying the viscosity and surface tension of the liquid phase on microbubble size and size distribution (Parhizkar, et al. 2013). They showed that bubble diameter could be reduced down to approximately half of the capillary diameter, but that the minimum bubble diameter (~50 μm) was still too large for clinical use. Moreover, addition of viscosity-enhancers should be considered carefully in clinical formulations.

C. Multi-stage and hybrid devices for microbubble production

Approaches relying on a two-stages microbubble production process have also been proposed, whereby larger precursor bubbles are produced in a first step, and their size is subsequently reduced down to clinically-applicable levels in a second step. Given the larger size of the precursor bubbles, it is possible to utilise channels of larger dimensions compared to microfluidic devices relying on a single-step microbubble production process. For example, Gnyawali *et al.* employed a 20 μm flow focusing orifice to produce bubbles of ~100 μm diameter, which were then conveyed through a serpentine shaped channel around which a negative pressure was applied (Gnyawali, et al. 2017). As the bubbles traversed this channel, the generated vacuum drove gas out of the bubbles, which in turn shrunk down to a useable clinical range of 1-7 μm in diameter. Microbubbles were stable at atmospheric pressure for at least 25 minutes, although their acoustic response or handling stability were not reported. Additionally, as each large precursor bubble generates only a single microbubble, the microbubble concentration in the end-product is likely to be low. Finally, the gas within the microbubbles may be irreversibly lost without some form of scavenging, which may be problematic if an expensive and/or polluting gas (e.g., sulphur hexafluoride) is employed as the microbubble core.

A further two-step approach that has been explored for microbubble production relies on the sonication of precursor bubbles induced by low-frequency ultrasound waves. Its implementation has been reported in a study by Chen *et al.* Large gas bubbles were firstly conveyed through an 860 μm (inner diameter) polyethylene tube to form a gas-in-liquid slug flow regime, with the fluid containing ~100-300 nm diameter ethyl cellulose particles. They subsequently travelled in front of a 20 kHz ultrasonic horn, externally coupled to the capillary, causing cavitation to occur at the interface between the gas bubbles and the particle-rich fluid. Cavitation resulted in the formation of microbubbles, which were stabilised by adsorption of the nanoparticles onto the gas-liquid interface. microbubble size dispersity could be reduced by increasing the sonication power, but it still encompassed a broad diameter range (i.e. from approximately 5 to 60 μm) (Chen, et al. 2014). The microbubble size distribution with the lowest dispersity had a peak diameter of ~20 μm, which is beyond the accepted limit for intravenous administration. Furthermore, the fluid temperature was observed to increase up to 80°C within 7 minutes of sonication, which may hinder the applicability of this method to the production of microbubbles loaded with bioactive compounds. However, compared to the approach by (Gnyawali, et al. 2017), this method enables production of multiple microbubbles from a single precursor bubble and therefore presents greater scalability potential. A summary of the microbubble sizes, polydispersity and production rates reported for published device is shown in Table 1 to show the key advances in size control and/or production rate.

Ohl *et al.* developed a T-junction microfluidic device coupled with a piezoelectric element, to investigate the behaviour of a gas–liquid interface exposed to ~100 kHz continuous ultrasound waves. It was shown that these interfaces develop standing surface waves, the amplitude of which depended upon the driving acoustic intensity (Ohl, et al. 2010). Pronounced crests formed at sufficiently high intensity, resulting in the entrapment of small bubbles between neighbouring and coalescing crests. These bubbles in turn underwent inertial cavitation and fragmentation; however, their size was not

142 fully characterised. The study thus demonstrates that it is possible to design a microfluidic system
143 coupled with an ultrasound source, in which the amplitude of the ultrasound wave can modulate the
144 surface oscillation of larger precursor bubbles, potentially leading to the formation of smaller
145 micrometre-scale bubbles. It also demonstrates that, by designing the system to maximise the acoustic
146 energy within the microfluidic channels, heat losses can be minimised. A similar approach however,
147 has not yet been investigated for the production of coated microbubbles with clinically relevant
148 characteristics.

149 The aim of the present study was therefore to determine whether a hybrid sonication-
150 microfluidic (or 'sonofluidic') device could be used to produce microbubbles in the 1-2 μm diameter
151 range with a clinically acceptable size distribution (all bubbles < 5 μm), and with production rates and
152 microbubble stability comparable to those of batch methods.

Approximate MB mean diameter (μm)	**Polydispersity index immediately after manufacture**	**Maximum MB Production Rate (MBs/sec)**	**Primary MB shell constituent**	**Reference**
5	**< 2%**	10^6	Phospholipid	Hettiarachchi *et al.* 2007
4	**< 2%**	10^6	Phospholipid and protein	Seo *et al.* 2010
2	10-50%	10^6	Phospholipid	Peyman *et al.* 2012
5	Not cited	Not cited	Phospholipid	Gnyawali *et al.* 2017
2.5	3%	10^6	Phospholipid	van Elburg *et al.* 2021

153
154 Table 1: Summary of the microbubble sizes, polydispersity and production rates reported for
155 selected published microfluidic devices.
156

157

158

II. MATERIALS AND METHODS

A. Sonofluidic device for microbubble production

1. Operating principle

The sonofluidic device developed in this study relies on a two-stages process to produce coated gas microbubbles, as illustrated in Figure 1A. In the first stage, relatively large bubbles (~180 μm in diameter) with a narrow size distribution are generated from a simple T-junction channel architecture by a hydrodynamic pinch-off mechanism. In the second stage, bubbles are exposed to low-frequency ultrasound from a piezoelectric transducer coupled with the exit channel from the T-junction, which causes the large bubbles to 'release' a population of smaller microbubbles (with mean diameter typically of ~1-2 μm). This operating principle was selected on the basis of the following postulated benefits compared to more conventional microfluidic-based approaches: (i) multiple microbubbles can be produced from a single precursor bubble to enhance production rates; (ii) high acoustic energy density can be generated within the microfluidic channel whilst minimising heat losses, which enables both effective absorption of coating material at the gas-liquid interface as well as incorporation of thermolabile bioactive compounds; (iii) given the relatively large size of the precursor bubbles, the microfluidic channels can be manufactured using cost-effective, easy-to-perform, and scalable techniques, and devices can be operated at larger volumetric flow rates; and (iv) devices can be potentially integrated with detection systems for in-line quantification of microbubble size distribution.

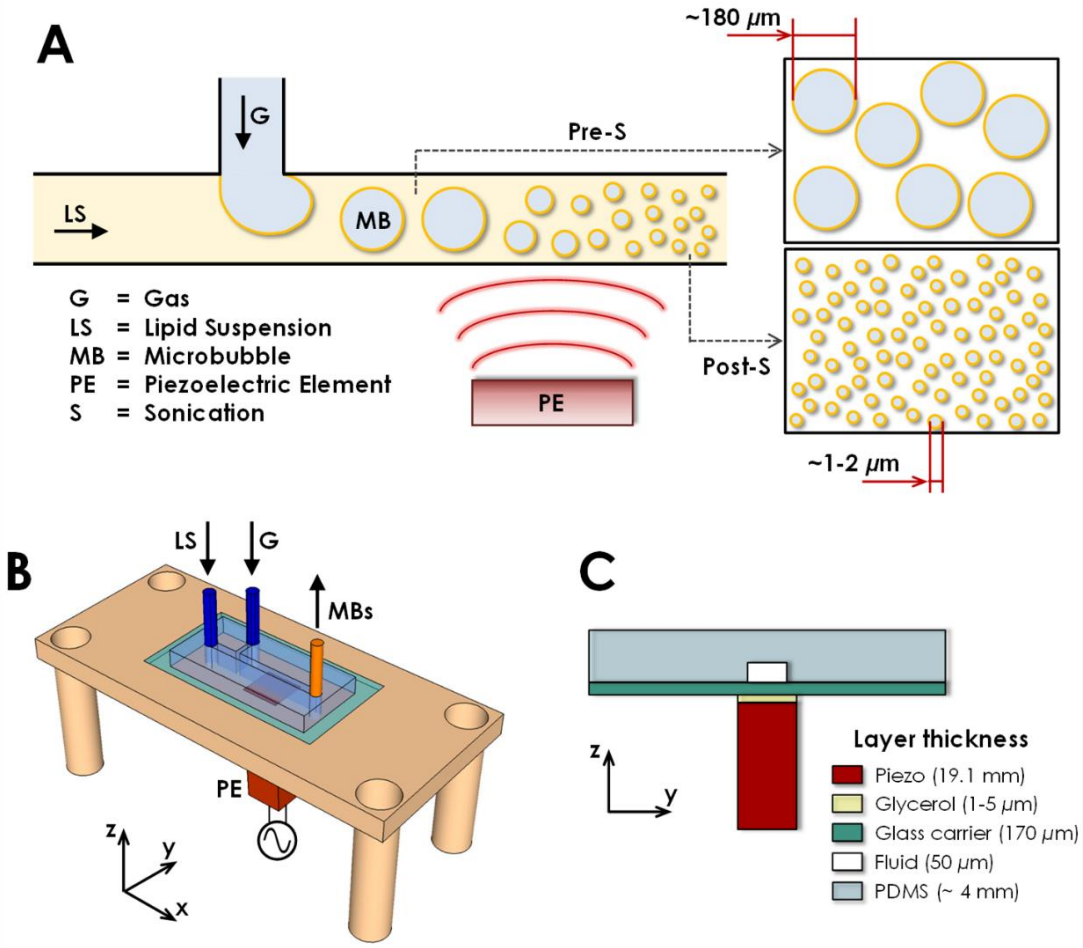

178

179 FIG. 1. (A) Schematic depiction of the operating principle governing microbubble generation within
180 the sonofluidic device. Larger bubbles (~180 μm in diameter) are produced using a T-junction
181 microfluidic architecture and exposed to a low frequency (in the range 71-73 kHz) ultrasound field,
182 causing the precursor bubbles to release smaller microbubbles (with mean diameter of ~1-2 μm). (B)
183 Schematic depiction of the overall sonofluidic device assembly. The microfluidic T-junction device
184 was positioned on to a custom-built holder, and coupled with a piezoelectric element (PE) generating
185 the ultrasound field. Flows of gas (G) and a lipid suspension (LS) were conveyed through the device
186 inlets, while the generated microbubble (microbubble) suspension was collected from the outlet. (C)
187 Cross-sectional view of the constitutive layers of the sonofluidic device, with indicated the
188 corresponding thickness for each layer. The ultrasound field was generated by a 19.1 mm thick

piezoelectric element (piezo), and travelled through a 0.17 mm thick glass carrier layer that was coupled to the piezoelectric transducer *via* a thin layer of glycerol (estimated thickness: 1 – 5 μm). It then propagated into the fluid layer of the microfluidic device (thickness: 50 μm), and subsequently through a ~4 mm thick layer of PDMS.

2. Device design, manufacturing and assembly

The microfluidic T-junction comprised two inlet and one outlet channels, with a rectangular cross-section (width × depth) of 250 μm × 50 μm (liquid suspension inlet and outlet) and 125 μm × 50 μm (gas inlet). This channel architecture was cast in poly(dimethylsiloxane) (PDMS, Sylgard^{TM} 184, Dow Inc., Michigan, USA) using a combined micromilling-replica moulding (μMi-REM) technique described previously (Carugo, et al. 2016). Briefly, the channel architecture was micromilled into a poly(methyl methacrylate) (PMMA, theplasticshop.co.uk, Coventry, UK) block to form a negative mould. A positive mould was manufactured by coating the milled PMMA mould with a bi-component epoxy adhesive (1:1 weight ratio between components, Yellow Dual Cartridge, RS Components Ltd., Corby, UK), which was then degassed by vacuum to remove entrapped air bubbles and left to cure at room temperature. After curing, the positive epoxy mould was removed from the PMMA block, and a 10:1 (w/w) mixture of PDMS and curing agent was poured over it and degassed for approximately 30 minutes to remove entrapped air bubbles. The PDMS layer was then cured overnight at room temperature. To complete the manufacturing process, the PDMS layer was removed from the positive epoxy mould and the patterned surface was activated by plasma treatment (using a plasma cleaner ATTO, Diener electronic GmbH, Ebhausen, Germany) along with a 74.00 mm × 49.00 mm × 0.17 mm (length × width × thickness) glass layer (Logitech, Glasgow, UK). After ~60-80 s of treatment, the PDMS layer was pressed firmly against the glass, and the assembly was heat treated on a hotplate set to 100°C for 10 minutes to achieve effective bonding between glass and PDMS. To create inlet

and outlet ports for the gas and liquid flows, 1/16" polyether ether ketone (PEEK) rods were glued by low-cost solvent-free glue (Pritt, Henkel Ltd., Herts., UK) onto the epoxy layer before PDMS pouring. The rods were then removed upon PDMS curing, prior to plasma treatment. After bonding to the glass surface, short segments of 3/32" OD Tygon® tubing (Cole-Parmer Instrument Co. Ltd., London, UK) were inserted into the ports to act as connectors for 1/16" OD tubing. These were connected to relevant syringes or gas circuits by 18G blunt needles (Sigma Aldrich, Gillingham, UK).

The PDMS device was then placed on to a custom holder (manufactured from polyoxymethylene), which contained a recess, in which the microfluidic device was positioned, and a central cut out window through which an ultrasound transducer was placed for coupling with the glass layer of the device (Figure 1B). Reversible coupling was achieved using a small volume of glycerol, which allowed for easy removal or replacement of the microfluidic device when required. The thin glass layer thus acted as an effective carrier for the ultrasound wave generated by the transducer, which was positioned 5 mm away from the junction between inlet channels. PDMS has a comparable characteristic acoustic impedance to the one of water (Carugo, et al. 2015, Leibacher, et al. 2014), it was therefore anticipated that ultrasound reflections at the liquid-PDMS interface would be minimised. The ultrasound transducer consisted of a single piezoelectric element (9.0 mm × 9.0 mm × 19.1 mm, Pz26, Meggitt PLC, UK) with a fundamental thickness resonance frequency of 69 kHz. Figure 1C shows a cross-sectional view of the constitutive layers of the sonofluidic device, in the region where the transducer is coupled with the glass layer, with the corresponding thickness values indicated for each layer.

3. Electronic components and ultrasound actuation methods

The transducer was driven in continuous mode by a 55 dB RF power amplifier (1040L, E&I, Rochester, NY, USA) fed from a signal generator (Agilent 33220A, Keysight Technologies, Santa Rosa, USA). Two different actuation methods were used in the present study, namely single frequency (SF) and frequency modulation (FM). In the latter method, a linear frequency sweeping was applied,

and the effects of varying both the frequency range and sweep period (or duration) on microbubble characteristics were investigated.

B. Microbubble Formulations

Phospholipids were selected as the primary microbubble coating material in this study, as they are the most commonly used shell constituent in commercial contrast agents (e.g., SonoVue®, Sonazoid® and Definity®) (Frinking, et al. 2020). The lipids 1,2-distearoyl-sn-glycero-3-phosphocholine (DSPC, 850365), 1,2-dipalmitoyl-sn-glycero-3-phosphocholine (DPPC, 850355) 1,2-Dipalmitoyl-sn-glycero-3-phosphatidic acid sodium salt (DPPA, 830855), 1,2-distearoyl-sn-glycero-3-phosphoethanolamine-N-[methoxy(polyethylene glycol)-5000] (DSPE-mPEG5000, 880220) and 1,2-dipalmitoyl-sn-glycero-3-phospho-(1'-rac-glycerol) (DPPG, 840455) were purchased as a 25 mg/mL solution in chloroform or powders from Avanti Polar Lipids, Inc. (Alabaster, AL, USA). Two different formulations of the microbubble shell were investigated, corresponding to: (i) a mixture of DSPC and polyoxyethylene (40) stearate (PEG-40S), which is a composition widely used in research settings (Borden, et al. 2005, Owen, et al. 2018); and (ii) a mixture of DPPC, DSPE-mPEG5000, and DPPA, which is comparable to the formulation of the clinically approved Definity® microbubbles (Lantheus Medical Imaging, MA, USA) (Segers, et al. 2017). In the first formulation, DSPC (25 mg/mL in chloroform) and PEG-40S (10 mg/mL in chloroform) were mixed in a glass vial to form a chloroform solution at a molar ratio of 9:1, respectively. In the second formulation, DPPC (25 mg/mL in chloroform), DSPE-mPEG5000 (25 mg/mL in chloroform) and DPPA (1 mg/mL in a chloroform, methanol and water mix) were mixed in a glass vial to a 20 mg total of lipid constituents at a molar ratio of 8:1:1, respectively. Chloroform solutions were covered with perforated Parafilm® (Bemis Company, Inc., Neenah, WI, USA) and allowed to evaporate overnight to form a homogenous lipid film. 10 mL Milli-Q water (Merck Millipore, Watford, UK) or a water, glycerol and propylene glycol mixture (80:10:10 v/v respectively) was added to the DSPC or Definity®-like lipid films, respectively. In the case of the

DSPC-based formulation, three different DSPC concentrations in the final suspension were investigated, corresponding to 2, 4 and 6 mg/mL, to assess whether lipid concentration had an effect on the characteristics of microbubbles produced using the sonofluidic device. The lipids were resuspended into the solvent by stirring at 100°C on a magnetic stirrer hotplate for a minimum of 30 minutes. They were then homogeneously dispersed within the solution by sonication for approximately 2.5 minutes using a micro-sonicator tip fully immersed in the solution at a power setting of 2 to 3 (Microson XL 2000, QSonica, Newtown, CT, USA).

C. Experimental procedures

Microbubbles produced using the sonofluidic device were compared with those produced by conventional sonication in terms of their size, stability, and concentration. In addition, the effect of changing the sonofluidic device driving ultrasound parameters was investigated, and performance consistency across multiple devices was assessed. Finally, different lipid formulations and concentrations were investigated.

1. Production of lipid microbubbles by conventional sonication

After resuspension and dispersion of lipids into the solvent, the sonicator tip was placed at the air-liquid interface and the headspace in the vial filled with nitrogen gas. The solution was sonicated under constant nitrogen flow for 30 seconds at a power setting of 14, to form a suspension of microbubbles. The suspension was left to cool to room temperature over 5 minutes. Typically, clinical microbubble formulations use heavy gases such as perfluorobutane or sulfur hexafluoride, but to facilitate a large number of experiments, nitrogen (supplied by BOC Gases, Guildford, UK) was used in this study.

2. Production of lipid microbubbles using the sonofluidic device

The device channels were flushed with ethanol and deionised water multiple times prior to use. The resuspended, fully dispersed lipid solution was transferred to a 10 mL syringe and connected to the liquid inlet port of the device. The gas inlet was connected to a nitrogen cylinder *via* a dual stage regulator with cut-off valve and an inline electronic pressure manometer (2023P Digitron, Elektron Technology, Cambridge, UK). A syringe pump (World Precision Instruments Inc., Florida, USA) was used to vary lipid flow rates into the device, whilst gas pressure control was supplied by the regulator. The device was run for one minute to establish a stable 'pinch-off' regime at the T-junction, indicated by the appearance of a steady stream of large bubbles. This regime was achieved at a volumetric flow rate of the lipid suspension of 0.5 mL/min and a nitrogen inlet pressure of 37 kPa. The mean diameter of the produced bubbles was approximately 180 μm, determined through optical microscopy of the collected bubble suspension (please see below). Upon formation of a steady bubble flow, the ultrasound transducer was actuated, which resulted in the production of smaller microbubbles. These were also collected from the outlet tube for microscopic analysis.

3. Microbubble concentration, size and stability analysis

Sonicated microbubbles were homogeneously dispersed by gentle manual agitation of the vial, and 10 μL of the suspension were loaded on a coverslip-covered haemocytometer *via* a pipette. The continuous-flow format of the sonofluidic device meant that the outlet tube could be directly connected to the hemocytometer chamber. Microbubbles were imaged using a brightfield microscope (Leica Microsystems GmbH, Wetzlar, Germany), and images were acquired using a digital camera (MicroPublisher 3.3 RTV, QImaging, Surrey, Canada). A 4× or 40× objective was used for imaging the larger precursor bubbles (~180 μm mean diameter) and smaller microbubbles (~1-10 μm diameter), respectively. Microbubble size and concentration were determined using a purpose-written image processing program in MATLAB (The Mathworks Inc., Natick, MA, USA), as previously described in Sennoga *et al.* (Sennoga, et al. 2012). A minimum of twenty images were analysed for each

sample. For stability analysis, microbubble size and concentration were measured as described every 10 minutes from the same sample. This was repeated three times using a fresh bubble suspension created from a new lipid film each time. The average microbubble mean diameter values reported in this manuscript are accompanied by the corresponding average standard deviation of the diameter distribution, which provides a quantification of microbubble size dispersity. Experiments were performed at the ambient room temperature (~18-22°C) and pressure. The microscope lamp was switched off in between measurements to avoid excessive heating of the sample, and the coverslip was left in place on the haemocytometer throughout.

4. Optimisation of sonofluidic device operating parameters

The effects of varying the sonofluidic device operating ultrasound parameters on microbubble production rate and size distribution were investigated. Parameters included the acoustic energy (e.g., by changing the input driving voltage to the amplifier in the range 300 – 900 mV), the frequency value in single frequency operation mode (in the range 67 – 76 kHz), and the sweep frequency range (between 69 kHz and 73 kHz) and period (in the range 1 – 1000 ms) in frequency modulation mode. Optimal operating parameters were identified, which provided the greatest production rate whilst retaining a clinically relevant mean microbubble diameter (of ~1-2 μm) and a low size dispersity.

5. Reproducibility of the sonofluidic device

To test the performance reproducibility of the sonofluidic device, three devices of the same design were constructed and run at the optimal ultrasound settings. Microbubbles in these experiments were produced using three independent lipid suspensions of DSPC:PEG40s (9:1 molar ratio).

D. Sonofluidic device for scaled-up microbubble production

A modified design of the sonofluidic device was developed to perform a preliminary investigation of whether microbubble production rates could be scaled-up by increasing both the microfluidic

device cross-sectional dimensions (and thus the operating flow rates) and the ultrasound field intensity. This scaled-up sonofluidic device was designed, manufactured, and operated following the same principles and procedures reported above. The ultrasound transducer was changed to a 60 kHz piezoelectric element (maximum power: 30 W, PZT-4, Beijing Ultrasonic, China), and the glass layer to a thicker 75 mm × 25 mm × 1 mm (length × width × thickness) slide to effectively sustain the greater levels of ultrasound-induced strain. The fluidic channels of the T-junction architecture had increased cross-sectional dimensions (width × thickness) of 1.0 × 0.1 mm (liquid suspension inlet and exit channels) and 0.5 × 0.1 mm (gas inlet channel). In the experiments using this scaled-up device, the ultrasonic transducer was driven at a peak-to-peak voltage (post amplification) of 200 V and the driving frequency was linearly swept between 60 and 62 kHz. These ultrasound settings were maintained constant throughout the experiments, while the volumetric flow rate of the lipid suspension was increased from 5 to 35 mL/min. The gas inlet pressure was manually adjusted as the liquid flow rate was increased, in order to maintain a stable stream of precursor bubbles forming at the junction between inlet channels. The lipid suspension in these experiments comprised DSPC and PEG40S at a molar ratio of 9:1, suspended in a water, glycerol and propylene glycol mixture (80:10:10 v/v respectively). The microbubbles size and concentration were determined by optical microscopy, following the protocol described above.

III. RESULTS AND DISCUSSION

A. Optimisation of sonofluidic device operating parameters

Figure 2 shows representative diameter distributions of phospholipid-coated (DSPC:PEG40S) precursor bubbles (i.e., not exposed to the ultrasound field) and the microbubbles generated upon activation of the piezoelectric transducer. Precursor bubbles formed at the T-junction by a pinch-off mechanism, and had a mean diameter of 181 μm and standard deviation of the distribution of 34 μm (Figure 2A), corresponding to a polydispersity index (PDI) of 0.035. Once exposed to the ultrasound

353 field, they formed microbubbles with a size distribution having mean diameter of 1.45 μm and
354 standard deviation of 0.76 μm (Figure 2B), corresponding to a PDI of 0.27.

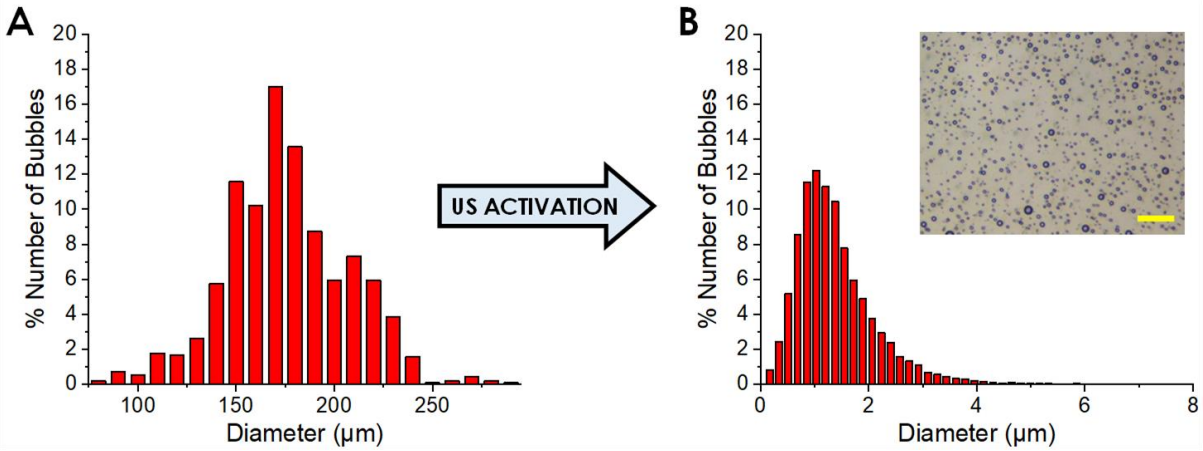

355

356 FIG. 2. Representative percentage weighted size distributions of (A) bubbles prior to activation of the
357 piezoelectric transducer (based on 20 images of ~1000 bubbles), and (B) microbubbles generated
358 upon activation of the ultrasound field (based on 30 images of ~13000 bubbles). The inset shows a
359 representative microscope image of microbubbles produced using the sonofluidic device (scale bar:
360 10 μm).

361 In order to determine the optimal operating parameters for the device, the driving ultrasound
362 frequency, amplitude, and frequency sweep settings were all varied. In a first series of experiments,
363 the transducer was driven in SF mode, and the effect of varying the ultrasound frequency was
364 investigated. Frequency values evaluated were equal to 67, 69, 71, 73 and 76 kHz, at a constant pre-
365 amplifier input voltage of 900 mV (see Figure 3A). It was found that increasing the ultrasound
366 frequency from 67 kHz to 69 kHz resulted in an increase in microbubble concentration (from 0.43 ±
367 0.06 × 10^8 microbubbles/mL to 1.05 ± 0.33 × 10^8 microbubbles/mL) and a slight decrease in
368 microbubble mean diameter and size dispersity (from 2.19 ± 1.28 μm to 1.90 ± 1.02 μm). A similar
369 trend was observed when the frequency was further increased from 69 kHz to 71 kHz (microbubble
370 concentration: 1.99 ± 0.25 × 10^8 microbubbles/mL; mean microbubble diameter: 1.56 ± 0.83 μm).

However, microbubbles produced at 73 kHz had comparable mean diameter and size dispersity (1.54 ± 0.79 μm) to those produced at 71 kHz, and only a slightly reduced concentration (1.69 ± 0.29 × 10^8 microbubbles/mL). Further increasing the driving frequency to 76 kHz caused a marginal increase in both microbubble size (mean diameter: 1.90 ± 1.35 μm) and concentration (1.88 ± 0.49 × 10^8 microbubbles/mL), but this was accompanied by an increase in the corresponding standard deviations. In a second series of experiments, the transducer was operated by applying a linear frequency modulation over a range of driving frequencies that excluded those values that resulted either in the lowest microbubble production rate (67 kHz) or the greatest variability in microbubble concentration and size (76 kHz). The sweep frequency ranges investigated were 69-73 kHz, 70-72 kHz, and 71-73 kHz, at a constant sweep period of 50 ms. Among the different modulation regimes evaluated, the 71-73 kHz sweep range resulted in the greatest microbubble concentration (3.22 ± 0.69 × 10^8 microbubbles/mL), corresponding to a production rate of approximately 2.7 × 10^6 microbubbles/s, and a clinically viable mean diameter of 1.45 ± 0.79 μm, and was thus selected as the preferred operating condition for subsequent tests. Operating the device in frequency sweeping also brings with it additional benefits, such as reduced temperature sensitivity, less requirements for controlling the ultrasound frequency (i.e., through automated frequency tracking methods), and potentially greater uniformity of the acoustic field within the fluid layer, as previously reported for other acoustofluidic devices (Carugo, et al. 2014, Manneberg, et al. 2009) . It should be noted that the optimal driving frequencies did not include the nominal resonance frequency of the piezoelectric element (67 kHz), which could be due to the effect of coupling the transducer with the microfluidic device structure. In some cases, it could also be observed that the produced microbubbles weren't efficiently released from the device, potentially due to the 'trapping' effect of acoustic radiation forces. Future studies could thus evaluate a wider range of combinations of driving frequencies and inlet

volumetric flow rates, as well as the applicability of a pulsed ultrasound mode, to further optimise microbubbles production rate.

The effect of varying the amplitude of the operating ultrasound wave was subsequently investigated (see Figure 3B), at a frequency sweep range of 71-73 kHz and period of 50 ms. By varying the pre-amplifier input voltage from 300 mV to 500 mV resulted in a significant increase in microbubble concentration (from $0.82 \pm 0.16 \times 10^6$ to $0.52 \pm 0.39 \times 10^8$ microbubbles/mL) and a reduction in microbubble mean diameter and corresponding standard deviation (from 4.39 ± 2.41 μm to 2.06 ± 1.13 μm). When the input voltage was further increased to 700 mV, it was again observed an increase in microbubble concentration ($1.81 \pm 0.21 \times 10^8$ microbubbles/mL) and a corresponding reduction in both microbubble mean diameter and standard deviation (1.63 ± 0.89 μm). The observed effect of the ultrasound intensity on microbubble characteristics may be due to the fact that the gas-liquid interface of precursor bubbles underwent oscillations of greater amplitude at the higher ultrasound intensities, which resulted in more frequent entrapments and subsequent fragmentation events of smaller microbubbles, consistently with the observations by Ohl and co-authors (Ohl, et al. 2010). The relationship between driving voltage and microbubble properties was however non-linear, and a further increase in the pre-amplifier input voltage (up to 900 mV) did not cause significant changes in both microbubble concentration ($1.65 \pm 0.54 \times 10^8$ microbubbles/mL) and size (1.69 ± 0.87 μm). Whilst input voltages of 700 mV and 900 mV led to comparable microbubble characteristics, the latter was selected as the preferred operating voltage in order to accommodate for potential reductions in the acoustic energy within the device, i.e., due to fluctuations in environmental temperature, variabilities in the manufacturing process, or other factors. Results also suggest that varying the input voltage to the sonofluidic device may be an effective way of tuning the microbubble mean diameter, although careful consideration should be given to the corresponding reduction in microbubble concentration.

418 Subsequently, the effect of varying the sweep duration (or period) was also investigated (see
419 Figure 3C). The transducer was driven at a pre-amplifier input voltage of 900 mV, and the frequency
420 was linearly swept between 71 and 73 kHz over a period of either 1, 5, 50, 250, 500, and 1000 ms.
421 Interestingly, the highest microbubble concentrations were generated at 1 ms and 1000 ms sweep
422 duration ($1.66 \pm 0.81 \times 10^8$ microbubbles/mL and $2.52 \pm 0.35 \times 10^8$ microbubbles/mL, respectively),
423 with a corresponding microbubble diameter of 1.73 ± 0.83 μm (1 ms) and 1.45 ± 0.76 μm (1000 ms).
424 Although there was no obvious relationship between microbubble characteristics and sweep period,
425 the greater production rate at the lowest sweep period (1 ms) may be due to the fact that precursor
426 bubbles were exposed to the optimal operating frequency for a longer period of time as they travelled
427 above the transducer, when compared to greater sweep periods (5 - 500 ms). The reasons behind
428 increased microbubble production rates at the highest sweep period (1000 ms) are not fully understood
429 yet, and merit further investigations. Previous studies using acoustofluidic resonators have shown that
430 frequency modulation can induce an oscillatory translational motion on particles or biological cells
431 suspended in a microfluidic cavity, and that the amplitude of oscillation scales with the sweep duration
432 (Ankrett, et al. 2013, Jonnalagadda, et al. 2018). It may thus be hypothesised that this enhanced
433 oscillatory motion may promote release of microbubbles from the gas-liquid interface of precursor
434 bubbles, overall resulting in greater microbubble concentrations in the end-product. Future studies
435 using ultra-high speed microscopy will be performed to gain a more pervasive understanding of the
436 effect of sweep duration on precursor bubble behaviour and microbubbles production mechanism.
437 Overall, the sonofluidic device operating parameters were chosen to be: a 71-73 kHz frequency
438 sweep over 1000 ms, at an input pre-amplification voltage of 900 mV, producing microbubbles of
439 mean diameter of ~1.45 μm and PDI = 0.27, at a production rate in the order of $\sim 2 \times 10^6$
440 microbubbles/s.

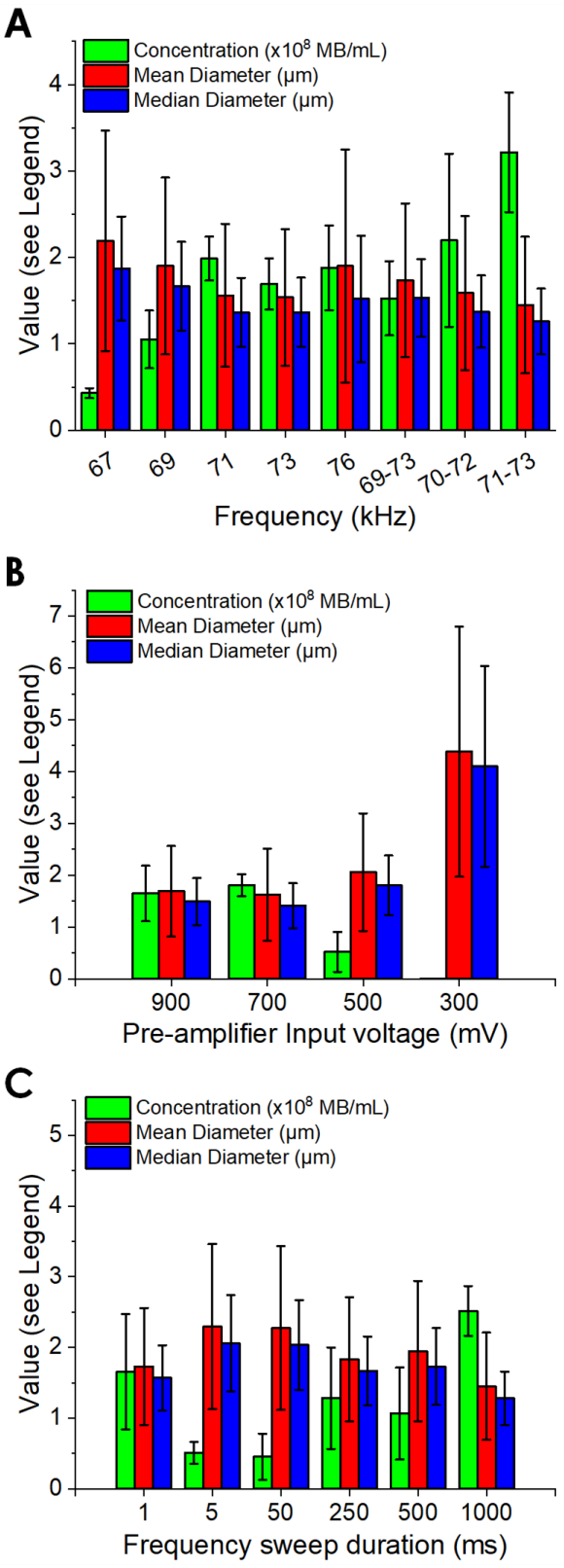
A
Concentration (x10^8 MB/mL)
Mean Diameter (µm)
Median Diameter (µm)
Value (see Legend)
0
1
2
3
4
67
69
71
73
76
69-73
70-72
71-73
Frequency (kHz)
B
Concentration (x10^8 MB/mL)
Mean Diameter (µm)
Median Diameter (µm)
Value (see Legend)
0
1
2
3
4
5
6
7
900
700
500
300
Pre-amplifier Input voltage (mV)
C
Concentration (x10^8 MB/mL)
Mean Diameter (µm)
Median Diameter (µm)
Value (see Legend)
0
1
2
3
4
5
1
5
50
250
500
1000
Frequency sweep duration (ms)

441

442

FIG. 3. (A) Effect of driving acoustic frequency on microbubble properties. The graph shows the population statistics of microbubbles generated at varying acoustic frequencies, at both single frequency and frequency modulation actuation modes. The piezoelectric transducer was operated at a pre-amplifier input voltage of 900 mV. The sweeping frequency groups (69-73, 70-72 and 71-73 kHz) used a linear frequency sweep over 50 ms. The optimum waveform frequency was chosen as a 71-73 kHz frequency sweep. n = 3 per frequency. The error bars indicate one standard deviation. (B) Effect of acoustic power on microbubble properties. The graph shows the population statistics of microbubbles generated at varying acoustic pre-amplifier input voltage. The piezoelectric transducer was run using a frequency sweep of 71-73 kHz over 50 ms. The optimum waveform pre-amplifier input voltage was chosen as 900 mV, although 700 mV provided microbubbles of comparable characteristics and would also be useable. n = 3 per input voltage. (C) The graph shows the effect of frequency sweep duration on microbubble properties. Population statistics of microbubbles generated at varying acoustic frequency sweep duration. The piezoelectric transducer was run using a frequency sweep of 71-73 kHz at pre-amplifier input voltage of 900 mV. The optimum waveform sweep duration was chosen as 1000 ms. n = 3 per frequency sweep, except 50 ms which is n = 2.

B. Sonofluidic device performance reproducibility

Three additional replicas of the microfluidic device were manufactured and run using the same piezoelectric transducer, to investigate performance reproducibility across different devices. Notably, the adopted reversible acoustic coupling enabled efficient removal and replacement of the microfluidic device units from the custom-built holder. Devices were all operated using a frequency sweep of 71-73 kHz over 1000 ms, at a pre-amplifier input voltage of 900 mV. The size and concentration of microbubbles produced with each device replica are reported in Figure 4 (Devices A, B, and C), together with those of the device previously utilised during performance optimisation tests (Device C, Figure 3C). The microbubble concentration varied in the range 1.76 - 3.77 $\times 10^8$ microbubbles/mL,

with an average between devices of 2.65 ± 0.83 × 10^8 microbubbles/mL. The mean microbubble diameter varied in the range 1.45 - 2.92 μm, and the average between devices was 2.34 ± 0.64 μm.

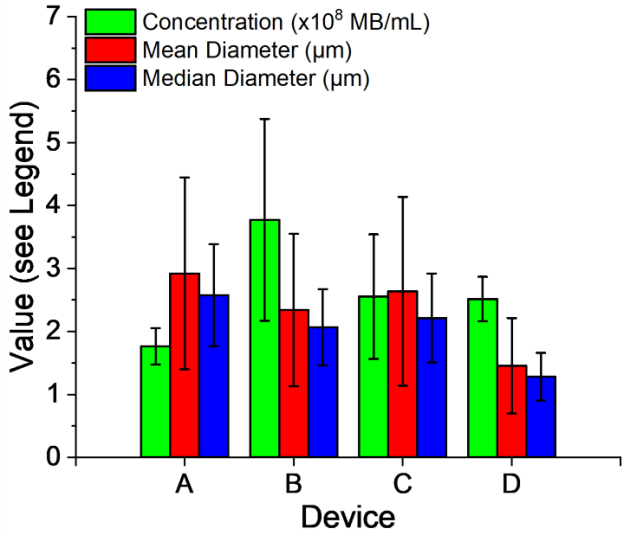

FIG. 4. Reproducibility of sonofluidic device performance. The graph shows the population statistics of microbubbles generated at a frequency sweep in the range 71-73 kHz over 1000 ms, at a pre-amplifier input voltage of 900 mV. In each group of experiments, a different microfluidic device was employed. The lipid formulation used was a 2 mg/mL DSPC:PEG40S. n = 3 per device.

Differences in performance between devices could be potentially attributed to discrepancies in the positioning of the piezoelectric element relative to the microfluidic channel architecture. This could be due to the nature of the manufacturing process, whereby the PDMS layer was manually bonded to the glass substrate. There may have also been differences in the thickness of the glycerol coupling layer between devices, which may have affected the acoustic energy field within the microfluidic channels. Moreover, using a commercial transducer with built-in case, may reduce performance sensitivity to changes in the environmental conditions. Overall, considering the cost-effective and easy-to-perform nature of the manufacturing method employed in this study, all sonofluidic device replicas were capable of producing phospholipid-shelled microbubbles at rates >10^6 microbubbles/s and with a clinically acceptable diameter.

C. Comparison with conventional batch sonication

DSPC:PEG40S (9:1) microbubbles were prepared both by batch sonication and using the sonofluidic device, and their size distribution and concentration were monitored over 30 minutes in a hemocytometer. The normalised average microbubble concentration and mean diameter are reported in Figures 5A and 5B, respectively. The microbubble suspensions produced by batch sonication had a larger initial mean diameter (2.65 μm) compared to those produced using the sonofluidic device (1.75 μm), and also contained microbubbles with diameter >10 μm. The concentration of microbubbles produced by batch sonication was greater than the ones produced using the sonofluidic device, but of the same order of magnitude (4.34×10^8 microbubbles/mL *vs.* 1.71×10^8 microbubbles/mL).

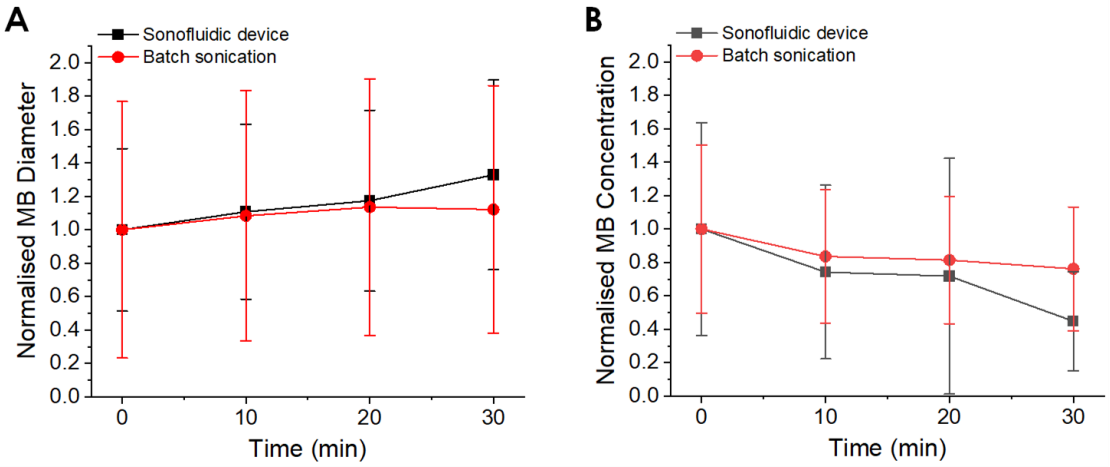

FIG. 5. Comparison of the stability of microbubbles produced by batch sonication and the sonofluidic device. Changes in (A) normalised mean diameter and (B) normalised concentration of microbubbles produced by sonication (red circles and line) and the sonofluidic device (black squares and line) over 30 minutes, measured from bright field microscope images. The sonofluidic device was operated using a frequency sweep in the range 71-73 kHz over 1000 ms, at a pre-amplifier input voltage of 900 mV. n = 3 per production method.

As shown in Figure 5, both types of microbubble underwent a comparable gradual decrease in concentration and increase in mean diameter over a period of 30 minutes. A two-sample *t*-test was performed on data pairs, and there were no statistically significant differences in microbubble properties between the two production techniques, suggesting that microbubbles produced using the sonofluidic device have comparable stability to those produced using conventional batch sonication.

D. Modification of microbubble formulation

The total lipid concentration of DSPC:PEG40S was varied in the range 2-6 mg/mL, to determine whether the amount of phospholipid had an effect on the characteristics of microbubbles produced using the sonofluidic device (see Figure 6). It was found that increasing the lipid concentration from 2 to 6 mg/mL increased microbubble concentration from $0.45 \pm 0.17 \times 10^8$ microbubbles/mL to $2.12 \pm 0.45 \times 10^8$ microbubbles/mL, likely due to the greater number density of phospholipid molecules readily available to stabilise the gas-liquid interface of the forming microbubbles. The increase in microbubble concentration was however less pronounced when the lipid concentration was varied from 4 to 6 mg/mL ($1.78 \pm 0.42 \times 10^8$ microbubbles/mL *vs.* $2.12 \pm 0.45 \times 10^8$ microbubbles/mL). The mean microbubble diameter did not show significant changes as a function of the total lipid concentration, and was in the range 1.67-1.99 μm. An alternative formulation, similar to that used in the commercial agent Definity®, was also tested using a 2 mg/mL total lipid concentration. microbubble shell constituents in this formulation were DPPC, DSPE-mPEG5000, and DPPA (at a molar ratio of 8:1:1). Unlike the DSPC:PEG40S microbubbles, the resuspension solvent was a more viscous solution of water, glycerol, and propylene glycol. The average microbubble concentration with this formulation was significantly greater than for DSPC:PEG40S, and equal to $7.79 \pm 2.43 \times 10^8$ microbubbles/mL (corresponding to an average production rate of 6.5×10^6 microbubbles/s). The mean microbubble diameter was slightly reduced when compared to the DSPC:PEG40s formulation with the same total lipid concentration (1.52 μm *vs.* 1.99 μm). These

observations are consistent with previous studies that reported an increase in microbubble concentration for DPPC-based formulations containing both glycerol and propylene glycol, and produced by mechanical agitation (Daeichin, et al. 2016). This is likely due to the reduced diffusivity of gas in the suspending medium as compared to saline, inhibiting microbubble destruction during processing; propylene glycol is also an effective de-foaming agent and this may help to promote formation of microbubbles over foam. A previous study by Parhizkar *et al.* also reported on an inverse relationship between diameter and medium viscosity, for microbubbles produced in a capillary embedded T-junction device (Parhizkar, et al. 2015). Moreover, the greater viscosity of the suspension medium in the Definity®-like formulation likely increased the overall microbubble lifetime.

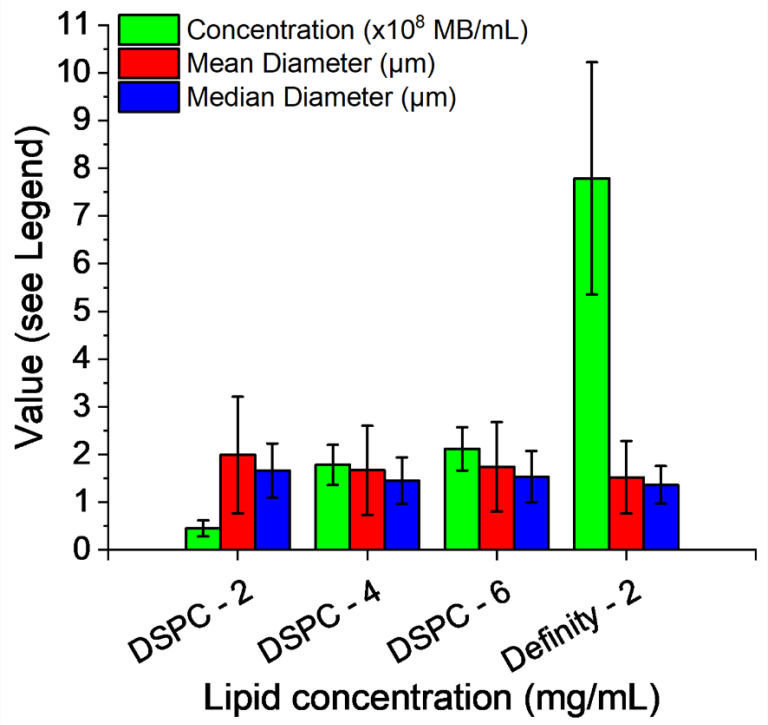

FIG. 6. Effect of total lipid concentration and formulation on the characteristics of microbubbles produced using the sonofluidic device. The graph shows the population statistics of microbubbles generated at a frequency sweep in the range 71-73 kHz over 1000 ms, at a pre-amplifier input voltage of 900 mV and using different lipid concentrations of DSPC:PEG40S and a Definity®-like

formulation. Optimisation of lipid concentration and formulation can improve microbubble production rates. n = 3 per formulation.

E. Demonstration of scaled-up microbubble production

Microbubbles were produced using the sonofluidic device described in section II.D, which consisted of a scaled-up microfluidic channel architecture operated at greater volumetric flow rates and driving acoustic power. The lipid suspension in these experiments comprised DSPC and PEG40S at a molar ratio of 9:1, suspended in a water, glycerol and propylene glycol mixture (80:10:10 v/v respectively). Notably, the microbubble production rate for this device directly correlated with the inlet flow rate, and increased from 0.18×10^8 microbubbles/s (at 5 mL/min) up to a maximum of 1.18×10^8 microbubbles/s (at 35 mL/min) for a single device, as shown in Figure 7A.

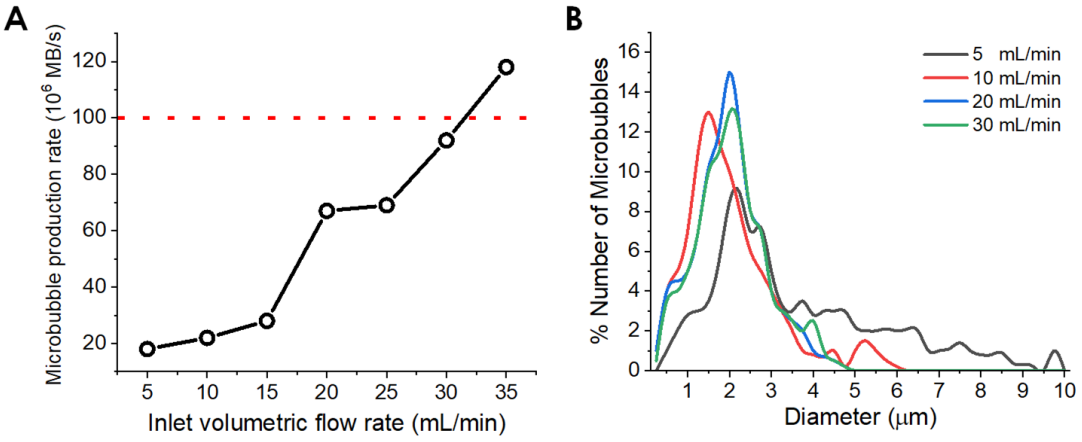

FIG. 7. (A) Microbubble production rate as a function of the inlet volumetric flow rate of the phospholipid suspension, obtained using the scaled-up sonofluidic device (driven using a 30 W transducer). The dotted red horizontal line corresponds to a production rate of 100 millions of microbubbles per second. (B) microbubbles size distribution at four different inlet volumetric flow rates. The lipid suspension in these experiments comprised DSPC and PEG40S at a molar ratio of 9:1, and the suspension medium was a mixture of water, glycerol and propylene glycol (80:10:10 v/v).

This corresponds to an increase of 1 to 2 orders of magnitude compared to the sonofluidic device configuration described above and other methods that have been published (Table 1). Volumetric flow rates >35 mL/min resulted in delamination of the PDMS from the glass substrate, and subsequent leakage. However, greater production rates may be achievable by improving the PDMS-glass bonding strength through optimisation of the plasma treatment process. As shown in Figure 7B, the microbubble size dispersity reduced with increasing the volumetric flow rate from 5 mL/min to 20 mL/min; however, it remained substantially unchanged at flow rates ≥ 20 mL/min. The greater size dispersity at the lower flow rates requires further investigations, but may be due to the increased transit time of precursor bubbles across the ultrasound field that may have potentially resulted in enhanced microbubble fragmentation and coalescence.

F. Limitations and future development for microbubble production

The results from this study demonstrate the feasibility of the proposed sonofluidic method as a means of producing microbubbles with a clinically relevant composition and size distribution, and in a continuous-flow format. The mechanism of microbubble formation was not explicitly investigated. It is hypothesised that standing surface waves were established at the gas-liquid interface of the larger precursor bubbles, and that the resulting surface oscillations led to the entrapment and 'release' of smaller microbubbles, consistent with the observations reported by Ohl *et al.* (Ohl, et al. 2010). Further work is required to test this hypothesis using high speed imaging as the device architecture and microbubble formulation are different.

To the best of the authors' knowledge, this is the first study reporting on the use of this approach to produce microbubbles stabilised with clinically relevant formulations of coating material, including a mimic of the clinically approved contrast agent Definity®. Compared to conventional batch sonication or other two-stage methods relying on ultrasound exposure of precursor bubbles (Chen, et al. 2014), the microbubbles produced using the sonofluidic device could be directly administered

580 intravenously without the need for post-production fractionation or centrifugation processes that are
581 typically required to eliminate microbubbles with diameter >10 μm. It will be necessary, however, to
582 confirm that the coating properties and acoustic response of the microbubbles are also comparable to
583 those of microbubbles produced via sonication.

584 The proposed sonofluidic strategy can produce microbubbles at rates of 10^8 per second using a
585 single channel, which is significantly greater than that achievable with conventional microfluidic
586 approaches and comparable to batch sonication. Production rates of $>10^9$ microbubbles per second
587 could easily be achieved through parallel actuation of multiple channels within a single platform; and
588 even higher rates using multiple devices. A further important point is that the risk of sample
589 contamination from erosion of the sonicator tip is also removed, as there is no direct contact between
590 the microbubble suspension and the ultrasound transducer as in batch sonication. This may be
591 advantageous for good manufacturing practice (GMP) compliance, and for producing microbubble
592 formulations loaded with bioactive compounds. The risk of clogging associated with conventional
593 microfluidic devices is also minimized and encapsulation efficiency expected to be significantly higher
594 than for conventional emulsification. This will likely be beneficial for the preparation of multi-
595 component bubbles, e.g. surface functionalised with targeting ligands or containing solid particles, for
596 which clogging is a greater risk. It would also be comparatively simple to add a secondary channel to
597 the device to facilitate subsequent reaction with a functional component. e.g. microbubbles could be
598 generated with a biotinylated lipid and then functionalised by exposing them to an avidin
599 functionalised drug molecule or targeting ligand. Production of functionalized microbubbles has yet
600 to be demonstrated, however, and this will be evaluated in future investigations, together with a
601 broader range of clinically applicable microbubble shell constituents.

602 There are other aspects of the developed system that also require improvement. These include (i)
603 the repeatability of the microfluidic device manufacturing process, and particularly of the relative

positioning of the PDMS and glass layers, (ii) the repeatability of the coupling process between the piezoelectric element and glass carrier, and (iii) the use of scalable and high volume capacity fluid supply units (e.g., pressurised reservoirs) as an alternative to syringe pumps. The results of this study also suggest that varying the input acoustic intensity may provide an effective means of controlling the microbubble size, although this may also result in a change in microbubble concentration. Future studies will investigate whether operating the device over a broader range of ultrasound frequencies (i.e., including harmonics of the transducer fundamental resonance frequency) would offer a method for tuning microbubble size and achieving a narrower size distribution.

IV. CONCLUSIONS

The feasibility of producing microbubbles with clinically relevant size (1-2 μm) and composition using a sonofluidic device was demonstrated. The microbubble diameter, concentration and stability were comparable with those achieved with batch sonication, but with a narrower size distribution and importantly no microbubbles larger than <5 μm in diameter. This removes the need for post-production fractionation. Production rates of $>10^8$ microbubbles per second were achieved using a single device. These are comparable with production rates associated with batch sonication, but the risk of contamination and/or degradation of sensitive components is removed. The device can also be operated continuously, reducing the risk of batch to batch variation. Further work is needed to elucidate the mechanism of microbubble formation within the device and to characterize the microbubble surface and acoustic properties.

ACKNOWLEDGEMENTS

This work was supported by the Institute of Engineering and Technology (AF Harvey Prize) and the Engineering and Physical Sciences Research Council (grants EP/I021795/1 and

EP/L025825/1). The authors gratefully acknowledge the help of Mr James Fisk in the University of Oxford workshop for assistance in device manufacturing.

REFERENCES

Al-Jawadi S, Thakur SS. Ultrasound-responsive lipid microbubbles for drug delivery: A review of preparation techniques to optimise formulation size, stability and drug loading. International journal of pharmaceutics 2020:119559.

Alter J, Sennoga CA, Lopes D, Eckersley RJ, Wells DJ. Microbubble stability is a major determinant of the efficiency of ultrasound and microbubble mediated in vivo gene transfer. Ultrasound in medicine & biology 2009; 35:976-84.

Ankrett DN, Carugo D, Lei J, Glynne-Jones P, Townsend PA, Zhang X, Hill M. The effect of ultrasound-related stimuli on cell viability in microfluidic channels. Journal of nanobiotechnology 2013; 11:1-5.

Borden MA, Kruse DE, Caskey CF, Zhao S, Dayton PA, Ferrara KW. Influence of lipid shell physicochemical properties on ultrasound-induced microbubble destruction. IEEE transactions on ultrasonics, ferroelectrics, and frequency control 2005; 52:1992-2002.

Browning RJ, Aron M, Booth A, Rademeyer P, Wing S, Brans V, Shrivastava S, Carugo D, Stride E. Spectral Imaging for Microbubble Characterization. Langmuir 2019; 36:609-17.

Carugo D, Lee JY, Pora A, Browning RJ, Capretto L, Nastruzzi C, Stride E. Facile and cost-effective production of microscale PDMS architectures using a combined micromilling-replica moulding (μMi-REM) technique. Biomedical microdevices 2016; 18:4.

Carugo D, Octon T, Messaoudi W, Fisher AL, Carboni M, Harris NR, Hill M, Glynne-Jones P. A thin-reflector microfluidic resonator for continuous-flow concentration of microorganisms: a new approach to water quality analysis using acoustofluidics. Lab on a Chip 2014; 14:3830-42.

Carugo D, Owen J, Crake C, Lee JY, Stride E. Biologically and acoustically compatible chamber for studying ultrasound-mediated delivery of therapeutic compounds. Ultrasound in medicine & biology 2015; 41:1927-37.

Castro-Hernández E, Van Hoeve W, Lohse D, Gordillo JM. Microbubble generation in a co-flow device operated in a new regime. Lab on a Chip 2011; 11:2023-29.

Chen H, Li J, Zhou W, Pelan EG, Stoyanov SD, Arnaudov LN, Stone HA. Sonication–Microfluidics for Fabrication of Nanoparticle-Stabilized Microbubbles. Langmuir 2014; 30:4262-66.

Daeichin V, van Rooij T, Skachkov I, Ergin B, Specht PA, Lima A, Ince C, Bosch JG, van der Steen AF, de Jong N. Microbubble composition and preparation for high-frequency contrast-enhanced ultrasound imaging: in vitro and in vivo evaluation. IEEE transactions on ultrasonics, ferroelectrics, and frequency control 2016; 64:555-67.

Dewitte H, Roovers S, De Smedt SC, Lentacker I. Enhancing nucleic acid delivery with ultrasound and microbubbles. *Nanotechnology for Nucleic Acid Delivery*: Springer, 2019. 241-51.

Dhanaliwala AH, Chen JL, Wang S, Hossack JA. Liquid flooded flow-focusing microfluidic device for in situ generation of monodisperse microbubbles. Microfluidics and nanofluidics 2013; 14:457-67.

Dollet B, van Hoeve W, Raven J-P, Marmottant P, Versluis M. Role of the channel geometry on the bubble pinch-off in flow-focusing devices. Physical review letters 2008; 100:034504.

Ferrara K, Pollard R, Borden M. Ultrasound microbubble contrast agents: fundamentals and application to gene and drug delivery. Annu. Rev. Biomed. Eng. 2007; 9:415-47.

Feshitan JA, Chen CC, Kwan JJ, Borden MA. Microbubble size isolation by differential centrifugation. Journal of colloid and interface science 2009; 329:316-24.

671 Frinking P, Segers T, Luan Y, Tranquart F. Three decades of ultrasound contrast agents: a review of the
672 past, present and future improvements. Ultrasound in medicine & biology 2020; 46:892-908.
673 Garg S, Thomas AA, Borden MA. The effect of lipid monolayer in-plane rigidity on in vivo microbubble
674 circulation persistence. Biomaterials 2013; 34:6862-70.
675 Garstecki P, Fuerstman MJ, Stone HA, Whitesides GM. Formation of droplets and bubbles in a
676 microfluidic T-junction—scaling and mechanism of break-up. Lab on a Chip 2006; 6:437-46.
677 Gnyawali V, Moon B-U, Kieda J, Karshafian R, Kolios MC, Tsai SS. Honey, I shrunk the bubbles:
678 microfluidic vacuum shrinkage of lipid-stabilized microbubbles. Soft Matter 2017; 13:4011-16.
679 Hettiarachchi K, Talu E, Longo ML, Dayton PA, Lee AP. On-chip generation of microbubbles as a practical
680 technology for manufacturing contrast agents for ultrasonic imaging. Lab on a Chip 2007; 7:463-
681 68.
682 Hosny NA, Mohamedi G, Rademeyer P, Owen J, Wu Y, Tang M-X, Eckersley RJ, Stride E, Kuimova MK.
683 Mapping microbubble viscosity using fluorescence lifetime imaging of molecular rotors.
684 Proceedings of the National Academy of Sciences 2013; 110:9225-30.
685 Jiang X, Zhang Y, Edirisinghe M, Parhizkar M. Combining microfluidic devices with coarse capillaries to
686 reduce the size of monodisperse microbubbles. RSC advances 2016; 6:63568-77.
687 Jonnalagadda US, Hill M, Messaoudi W, Cook RB, Oreffo RO, Glynne-Jones P, Tare RS. Acoustically
688 modulated biomechanical stimulation for human cartilage tissue engineering. Lab on a Chip
689 2018; 18:473-85.
690 Kooiman K, Vos HJ, Versluis M, de Jong N. Acoustic behavior of microbubbles and implications for drug
691 delivery. Advanced drug delivery reviews 2014; 72:28-48.
692 Leibacher I, Schatzer S, Dual J. Impedance matched channel walls in acoustofluidic systems. Lab on a
693 Chip 2014; 14:463-70.
694 Manneberg O, Vanherberghen B, Önfelt B, Wiklund M. Flow-free transport of cells in microchannels by
695 frequency-modulated ultrasound. Lab on a Chip 2009; 9:833-37.
696 Ohl S-W, Ow DS-W, Klaseboer E, Wong VV, Camattari A, Ohl C-D. Creation of cavitation activity in a
697 microfluidic device through acoustically driven capillary waves. Lab on a Chip 2010; 10:1848-55.
698 Owen J, Kamila S, Shrivastava S, Carugo D, Bernardino de la Serna J, Mannaris C, Pereno V, Browning R,
699 Beguin E, McHale AP. The Role of PEG-40-stearate in the Production, Morphology, and Stability
700 of Microbubbles. Langmuir 2018; 35:10014-24.
701 Pahlavan AA, Stone HA, McKinley GH, Juanes R. Restoring universality to the pinch-off of a bubble.
702 Proceedings of the National Academy of Sciences 2019; 116:13780-84.
703 Parhizkar M, Edirisinghe M, Stride E. Effect of operating conditions and liquid physical properties on the
704 size of monodisperse microbubbles produced in a capillary embedded T-junction device.
705 Microfluidics and nanofluidics 2013; 14:797-808.
706 Parhizkar M, Edirisinghe M, Stride E. The effect of surfactant type and concentration on the size and
707 stability of microbubbles produced in a capillary embedded T-junction device. Rsc Advances
708 2015; 5:10751-62.
709 Parhizkar M, Stride E, Edirisinghe M. Preparation of monodisperse microbubbles using an integrated
710 embedded capillary T-junction with electrohydrodynamic focusing. Lab on a Chip 2014; 14:2437-
711 46.
712 Peyman SA, Abou-Saleh RH, McLaughlan JR, Ingram N, Johnson BR, Critchley K, Freear S, Evans JA,
713 Markham AF, Coletta PL. Expanding 3D geometry for enhanced on-chip microbubble production
714 and single step formation of liposome modified microbubbles. Lab on a Chip 2012; 12:4544-52.
715 Rademeyer P, Carugo D, Lee JY, Stride E. Microfluidic system for high throughput characterisation of
716 echogenic particles. Lab on a Chip 2015; 15:417-28.

Rickel JR, Dixon AJ, Klibanov AL, Hossack JA. A flow focusing microfluidic device with an integrated Coulter particle counter for production, counting and size characterization of monodisperse microbubbles. Lab on a Chip 2018; 18:2653-64.
Segers T, Gaud E, Casqueiro G, Lassus A, Versluis M, Frinking P. Foam-free monodisperse lipid-coated ultrasound contrast agent synthesis by flow-focusing through multi-gas-component microbubble stabilization. Applied Physics Letters 2020; 116:173701.
Segers T, Lohse D, Versluis M, Frinking P. Universal equations for the coalescence probability and long-term size stability of phospholipid-coated monodisperse microbubbles formed by flow focusing. Langmuir 2017; 33:10329-39.
Sennoga CA, Yeh JS, Alter J, Stride E, Nihoyannopoulos P, Seddon JM, Haskard DO, Hajnal JV, Tang M-X, Eckersley RJ. Evaluation of methods for sizing and counting of ultrasound contrast agents. Ultrasound in medicine & biology 2012; 38:834-45.
Seo M, Gorelikov I, Williams R, Matsuura N. Microfluidic Assembly of Monodisperse, Nanoparticle-Incorporated Perfluorocarbon Microbubbles for Medical Imaging and Therapy. Langmuir 2010; 26:13855-60.
Sirsi S, Feshitan J, Kwan J, Homma S, Borden M. Effect of microbubble size on fundamental mode high frequency ultrasound imaging in mice. Ultrasound in medicine & biology 2010; 36:935-48.
Stride E, Edirisinghe M. Novel microbubble preparation technologies. Soft matter 2008; 4:2350-59.
Stride E, Saffari N. Microbubble ultrasound contrast agents: a review. Proceedings of the Institution of Mechanical Engineers, Part H: Journal of Engineering in Medicine 2003; 217:429-47.
Stride E, Segers T, Lajoinie G, Cherkaoui S, Bettinger T, Versluis M, Borden M. Microbubble agents: New directions. Ultrasound in medicine & biology 2020; 46:1326-43.
van Elburg B, Collado-Lara G, Bruggert GW, Segers T, Versluis M, Lajoinie G. Feedback-controlled microbubble generator producing one million monodisperse bubbles per second. Rev Sci Instrum 2021; 92.